Supporting Information

An Insoluble p-Type Organic Polymer Cathode with 9,9'-Bicarbazole Core for Highly Stable Li/Na/K-Based Dual-Ion Full Batteries

Kexin Fan[1], Huilin Ma[1], Wu Tang[1*], Wenjun Li[1], Shan Jia[1], Jiahui Hu[1], Xinyu Liu[1], Yuanhe Zhang[1] and Cong Fan[1*]

[1] School of Materials and Energy, University of Electronic Science and Technology of China (UESTC), Chengdu 611731, China

E-mail: tang@uestc.edu.cn; fancong@uestc.edu.cn

General information

All reagents commercially available were used as received. For example, phenazine, 3,6-dibromocarbazole, RuPhos (2-dicyclohexylphosphino-2',6'-diisopropoxybiphenyl) and RuPhos Pd G2 precatalyst were all from Shanghai Aladdin Bio-Chem Technology Co., Ltd. The carbon additives of Ketjen Black (KB) and Super P (SP) were provided by Lion Co. LTD. Polyacrylonitrile copolymer (La133), lithium hexafluorophosphate ($LiPF_6$), sodium hexafluorophosphate ($NaPF_6$), potassium hexafluorophosphate (KPF_6), ethylene carbonate/ethyl diethyl carbonate/dimethyl carbonate (EC/DEC/DMC), diethylene glycol dimethyl ether (DEGDME), and dimethyl ether (DME) were purchased from DoDo-Chem (China). The 500 MHz ^{1}H nuclear magnetic resonance (NMR) was performed on BRUKER-AVANCE-NEO600. The gel permeation chromatography (GPC) test was performed on PL-GPC220. The morphology images of the samples were collected by the field-emission scanning electron microscope (FE-SEM, Hitachi, S3400N). The ex-situ X-ray photoelectron spectroscopy (XPS) test was measured by the Thermo Scientific K-Alpha. The Fourier transform infrared spectrum (FT-IR) was recorded using KBr pellets on a Thermo Scientific Nicolet iS50 with the wavenumber range of 400-4000 cm^{-1}. The cyclic voltammetry (CV) test was measured by a CHI instrument electrochemical workstation (650E). All cells (CR2032) were assembled in the argon-filled glove box. The galvanostatic charge-discharge curves were collected by a CT2001A cell test instrument (LAND Electronic Co.) under room temperature. All the half and full cells were tested at room temperature (20-30 ^{o}C).

Synthesis of 3,3′,6,6′-tetrabromo-9,9′-bicarbazole (BCz-4Br)

BCz-4Br was synthesized according to the reported procedure.[1] To a solution of 3,6-dibromocarbazole (3.25 g, 10 mmol) in 100mL acetone was added slowly $KMnO_4$ (3.95 g, 25 mmol) at room temperature. The resulting mixed solution was heated under reflux at 60°C for 5 h. After cooling to room temperature, the solution was distilled under vacuum, the resulting reaction mixture was suspended in chloroform, filtered, and washed with chloroform. The filtrate was mixed with saturated aqueous $Na_2S_2O_3$ solution, saturated salt water, dried over $MgSO_4$, filtered, and concentrated under reduced pressure. The leached residue was purified by recrystallization from chloroform/ hexane to give the light orange powder (2.69 g, 83% yield). ^{1}H NMR (500 MHz, d_6-DMSO) δ (ppm): 8.72 (d, $J = 1.8$ Hz, 4H), 7.55 (dd, $J = 8.6$, 1.9 Hz, 4H), 6.91 (d, $J = 8.6$ Hz, 4H).

Synthesis of P(BCz4PZ)

5,10-dihydrophenazine was prepared according to the reported procedure.[2] Dihydrophenazine (364 mg, 2 mmol), 3,3′,6,6′-tetrabromo-9,9′-bicarbazole (BCz-4Br, 715 mg, 1.1 mmol), RuPhos ligand (14 mg, 0.03 mmol), RuPhos Pd G2 precatalyst (23 mg, 0.03 mmol) and t-BuONa (481 mg, 5.00 mmol) were added to a Schlenk tube. Under N_2 atmosphere, 20 mL toluene was added. The mixture was reacted at 110°C for 3 days. After cooling to room temperature, the resulting precipitate was filtered and washed with H_2O, methanol, CH_2Cl_2 and acetone, respectively. The obtained sample was further extracted by the Soxhlet method with chloroform and dried in vacuum oven at 80°C for 24 hours (502 mg, 73%).

GPC test of P(BCz4PZ)

The solution of P(BCz4PZ) sample in 1,2,4-trichlorobenzene at 150-200 °C was prepared and filtered by 0.20 μm PTFE membrane filters before measurement. And the polyethylene glycol with the defined molar mass was selected as standard sample. Subsequently, the polymer solution to be measured passed through a chromatographic column (PLgel Olexis) with different pore diameters, and the flow rate of the solution was 1 mL min^{-1}. Under the same test conditions, a corresponding relationship curve between elution volume or elution time and relative molecular mass was made by using standard polymers. A series of GPC standard spectra were obtained, corresponding to the retention times of samples with different relative molecular masses, and the resulting curve was called the "calibration curve". Through the calibration curve, the various required relative molecular mass and relative molecular mass distribution information could be calculated from the GPC

spectrum.

Half cells

The P(BCz4PZ)-based electrodes were fabricated by 60 wt% P(BCz4PZ), 30 wt% KB and 10 wt% La133 (binder). The neat loading mass of P(BCz4PZ) on Al foil was >2 mg cm^{-2}. The anodes were Li/Na/K metals, respectively. The electrolytes for Li/Na/K-based half cells were 1 M LiPF$_6$ in EC/DEC/DMC, 1 M NaPF$_6$ in DEGDME, and 1 M KPF$_6$ in DME, respectively. The separator was Whatman glass fiber/Celgard 2325. All half cells (CR2032) were assembled in the argon-filled glove box. CVs were tested at a scan rate of 0.1 mV s^{-1} between 2.5-4.3V (vs. Li$^+$/Li), between 2.5-4.2 V (vs. Na$^+$/Na) and between 2.5-4.2 V (vs. K$^+$/K) using electrochemical workstation (CHI 650e). All the capacities were reported based on the mass of P(BCz4PZ).

Full cells

The graphite (C) anodes were gained by mixing with La133 (10%), while the hard carbon (HC) anodes were obtained by blending with SP (10%) and La133 (10%). The resulting electrode slurry coated on Cu foil with average loading of 1.5-2 mg cm^{-2}. To remove the side reactions (solid-electrolyte interphase (SEI)) on the anode, all the carbon anodes were first tested for 2 cycles (at 100 mA g^{-1}) and stopped at the pristine state. Afterwards, the carbon-based half cells were subsequently disassembled in the Ar-filled glove box, and the anodes were taken out to fabricate full cells with the initial P(BCz4PZ) cathode. The electrolytes were 1 M LiPF$_6$ in EC/DEC/DMC, 1 M NaPF$_6$ in DEGDME, and 2 M KPF$_6$ in DME, respectively. The separators were Whatman glass fiber and Celgard 2325. The net capacity ratio between positive and negative electrode material was around 1:1.1. All cells (CR2032) were fabricated in an Ar-filled glovebox. Besides, the galvanostatic charge-discharge tests of the full cells was carried out in the voltage window of 2.4-4.2 V (P(BCz4PZ)IIC Li-based dual-ion full batteries), 2.4-4.1 V (P(BCz4PZ)IIHC Na-based dual-ion full batteries) and 2.1-4.0 V (P(BCz4PZ)IIC K-based dual-ion full batteries).

Energy density calculation

The energy densities of Li/Na/K-based dual-ion batteries can be calculated using the formula as follows:

$$E = \frac{It * V}{m(cathode) + m(anode) + m(anion) + m(M^+)}$$

$$m(anion) = \frac{It}{C_T(anion)}, m(M^+) = \frac{It}{C_T(M^+)}$$

Where It is the recorded capacity (mAh), V is the average discharge voltage (V) read from CT2001A cell test instrument, $m(cathode)$ is the mass of cathode, $m(anode)$ is the mass of anode, $m(anion)$ is the mass of anions (PF_6^-) inserted in the charge process, $m(M^+)$ is the mass of metal ions inserted in the charge process (M=Li/Na/K). For details: $C_T(C)$ is 370 mAh g^{-1} (in Li-based half cells), $C_T(HC)$ is 300 mAh g^{-1}, $C_T(C)$ is 200 mAh g^{-1} (in K-based half cells), $C_T(PF_6^-)$ is 185 mAh g^{-1}, and $C_T(M^+)$ is the specific capacity of Li$^+$ (3860 mAh g^{-1})/Na$^+$ (1165 mAh g^{-1})/K$^+$ (687 mAh g^{-1}) ions, respectively.

Table S1. The energy density calculation for the P(BCz4PZ)-based dual-ion full batteries.

	$E_{(cathode)}$	$E_{(cathode + anode + electrolyte)}$
Li: P(BCz4PZ)IIC	$\dfrac{115 * 3.29}{1}$	$\dfrac{115 * 3.29}{1 + (115/185) + (115/3860) + (115/370)}$
Na: P(BCz4PZ)IIHC	$\dfrac{122 * 3.3}{1}$	$\dfrac{122 * 3.3}{1 + (122/185) + (122/1165) + (122/300)}$
K: P(BCz4PZ)IIC	$\dfrac{122 * 2.8}{1}$	$\dfrac{122 * 2.8}{1 + (122/185) + (122/687) + (122/200)}$
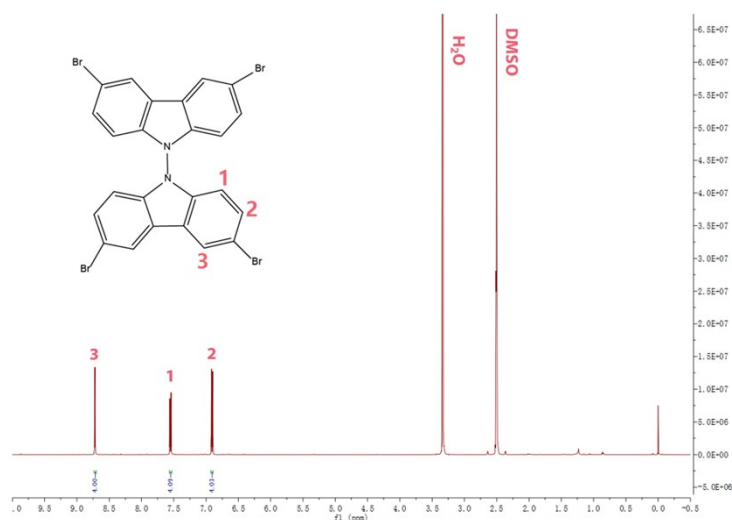
Figure S1. ^{1}H NMR spectrum for BCz-4Br in d$_6$-DMSO.
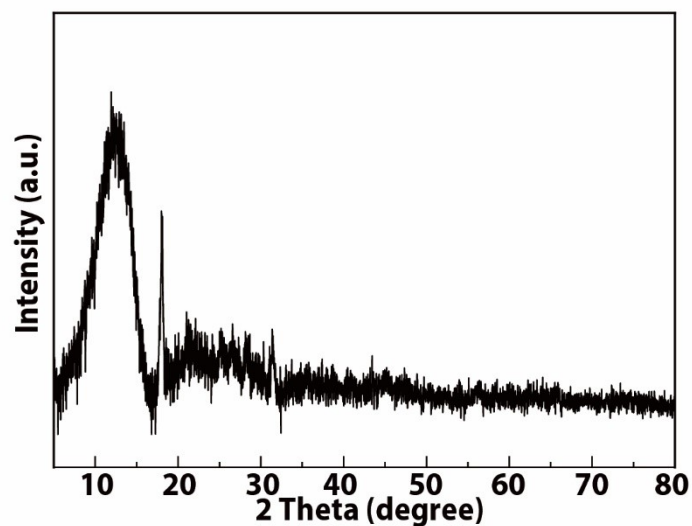
Figure S2. The XRD pattern of P(BCz4PZ).
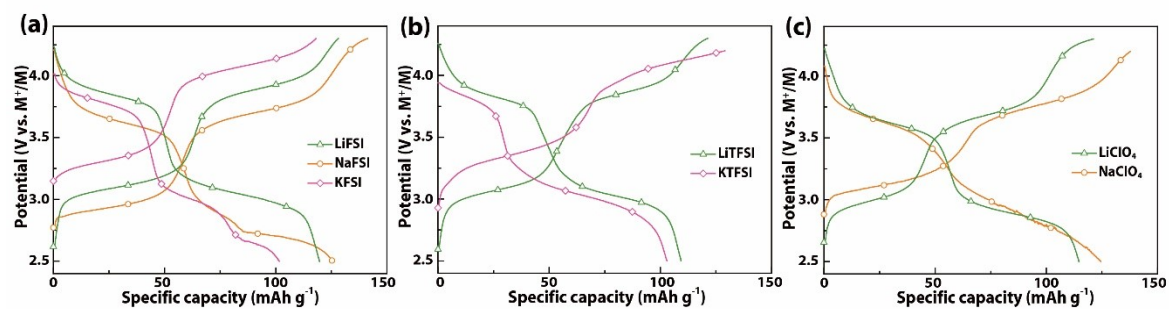
Figure S3. Electrochemical behavior of P(BCz4PZ) in different electrolytes. a) The charge-discharge curves of P(BCz4PZ) in LiFSI, NaFSI and KFSI-based electrolytes; b) The charge-discharge curves of P(BCz4PZ) in LiTFSI, and KTFSI-based electrolytes; c) The charge-discharge curves of P(BCz4PZ) in LiClO$_4$, and NaClO$_4$-based electrolytes.
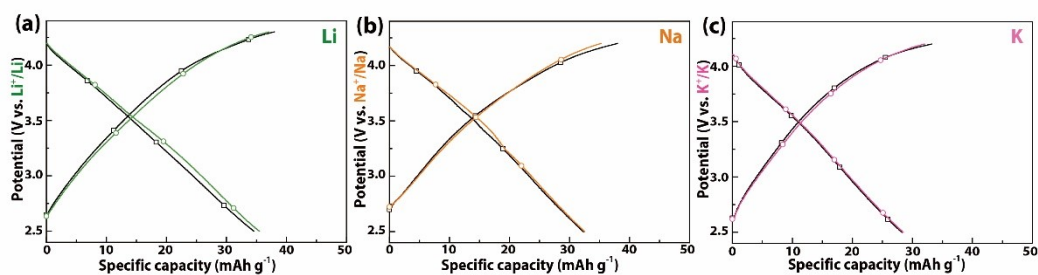
Figure S4. The charge-discharge profiles of the conductive carbon electrode (KB:La133=3:1 wt%) in Li/Na/K-based half cells, respectively.
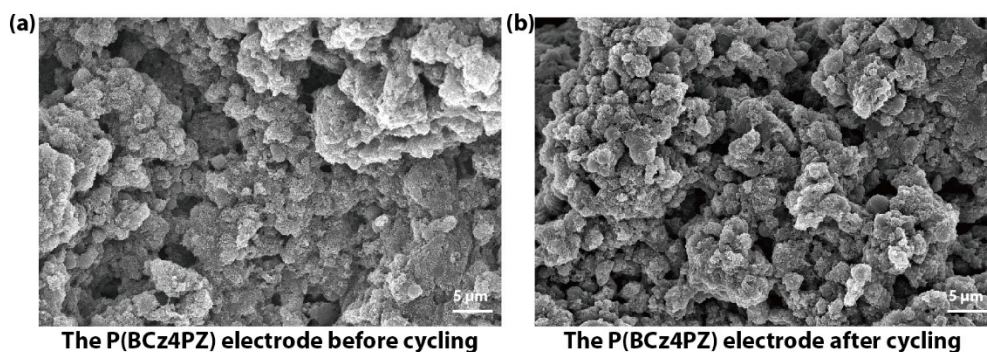
Figure S5. The SEM images of the P(BCz4PZ) electrodes before and after cycling in Li-based half cells.

GITT test

A constant current density of 0.5 C for 5 min and then relaxing for 30 min at open circuit (1 C corresponds to the current density of 160 mA g^{-1}) was exploited. Afterwards, the ion diffusion coefficients based on the GITT results were calculated using the following equation.

$$D = \frac{4}{\pi}(\frac{n_m V_m}{S})^2(\frac{\Delta E_s}{\tau(dE_\tau/d\sqrt{\tau})})^2 = \frac{4}{\pi}(\frac{V}{S})^2(\frac{\Delta E_s}{\tau(dE_\tau/d\sqrt{\tau})})^2 \approx \frac{4}{\pi\tau}(L)^2(\frac{\Delta E_s}{\Delta E_\tau})^2$$

In this equation, n_m is the mole number of the active materials; V_m is the molar volume of active materials; S is the effective area of the electrode (1.13 cm^2); τ is the relaxation time (1800 s); L is the average thickness of P(BCz4PZ) electrodes; $\triangle E_s$ is the potential change between neighboring relaxation end time; $\triangle E_\tau$ is the potential change caused by every constant current charge/discharge process.
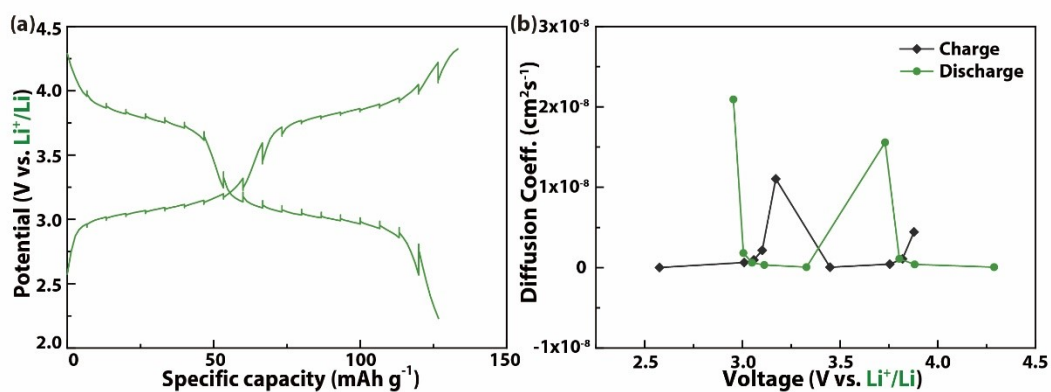
Figure S6. (a) The GITT curves of P(BCz4PZ) in Li-based half cells; (b) The realized ion diffusion coefficient for P(BCz4PZ) in Li-based half cells.

Cyclic voltammograms (CV) test at different scan rates

The reaction kinetics of P(BCz4PZ) electrode were analyzing according to the following equations:

$$i = av^b \qquad\qquad Equation\ 1$$
$$\log i = b\log v + \log a \qquad\qquad Equation\ 2$$

In the above equations where i is the peak current of six redox peaks, v is the sweep rates, a and b are adjustable parameters. The b value could be acquired through the slope of linear fitting results in the log plot between peak current and scan rates. If b value is 0.5, the electrode is dominated by diffusion (battery behavior), whereas the process is capacity-controlled (capacity behavior) when the b value is close to 1. Notably, when the b value exists between 0.5 and 1, the electrode kinetics are the hybridization of diffusion and capacitive behavior. The capacitive contribution can also be measured according to the equations below:

$$i = k_1 v + k_2 v^{1/2} \qquad\qquad Equation\ 3$$
$$i / v^{1/2} = k_1 v^{1/2} + k_2 \qquad\qquad Equation\ 4$$

k_1 and k_2 are two variables, which were only related to the potential under the condition of negligible voltage polarization change between various scan rates.
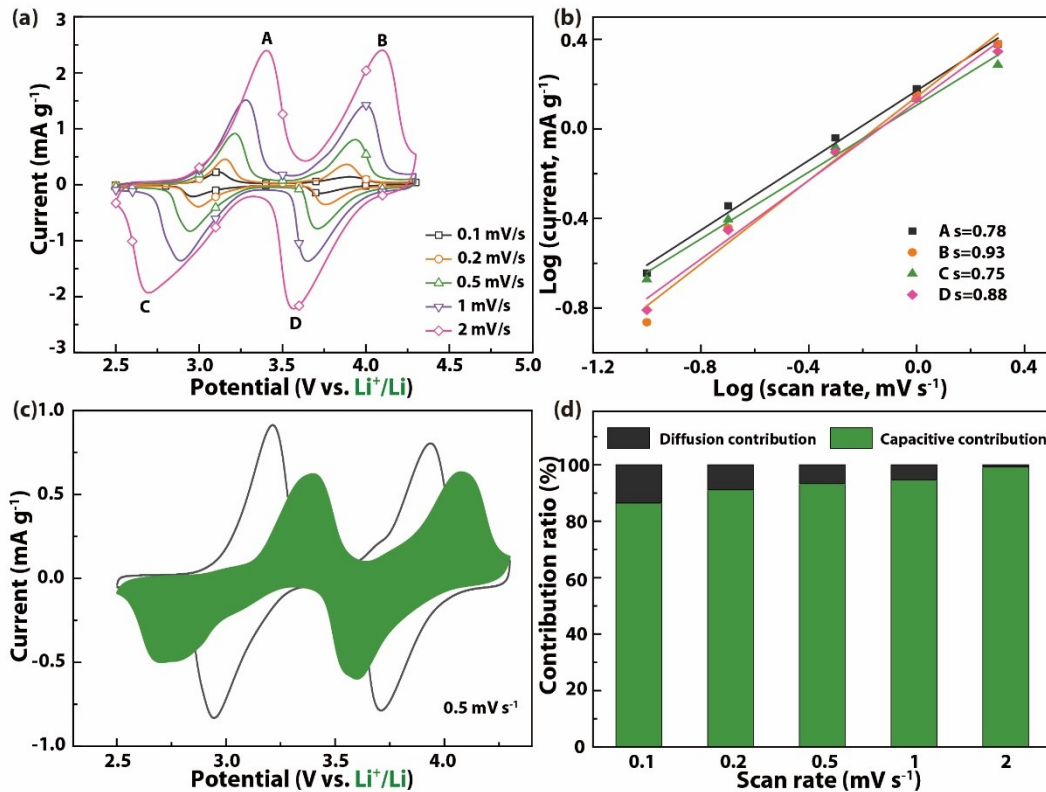
Figure S7. (a)The CV curves of P(BCz4PZ) at different scan rates from 0.1 to 2 mV s^{-1} in Li-based half cells; (b) The linear fitting results of logarithm (log) relationship between peak current and different scan rates; (c) The pseudocapacitance contribution at 0.5 mV s^{-1} for P(BCz4PZ); (d) The pseudocapacitance contribution at various scan rates.
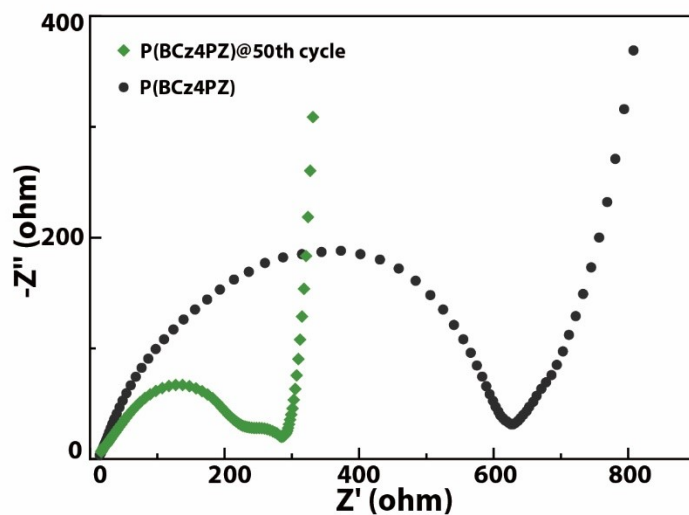
Figure S8. The EIS tests for P(BCz4PZ) before and after cycling in Li-based half cells.
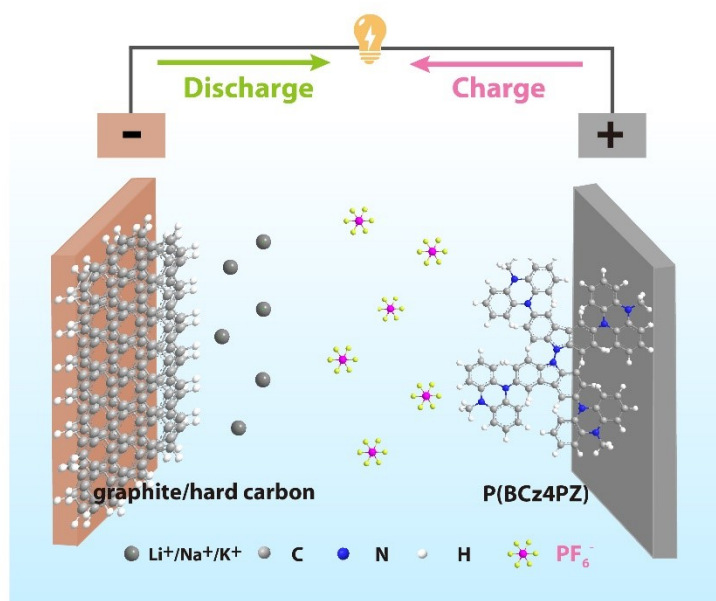
Figure S9. The configuration and mechanism of the Li/Na/K-based dual-ion full batteries.
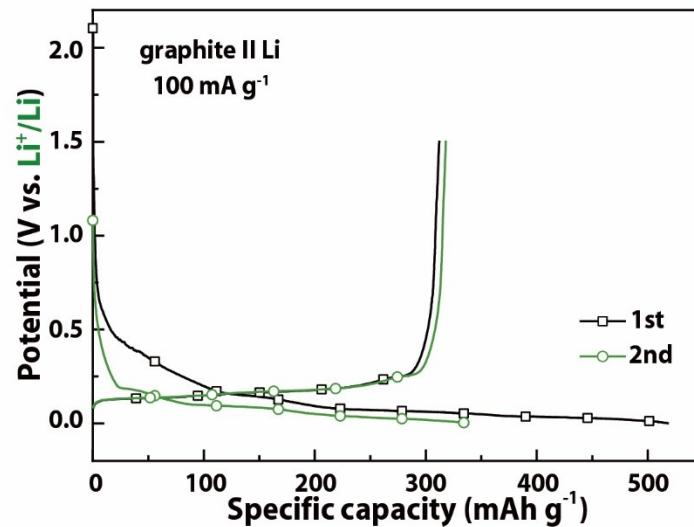
Figure S10. The charge-discharge curves of graphite in Li-based half cells in 0.001-1.5 V.
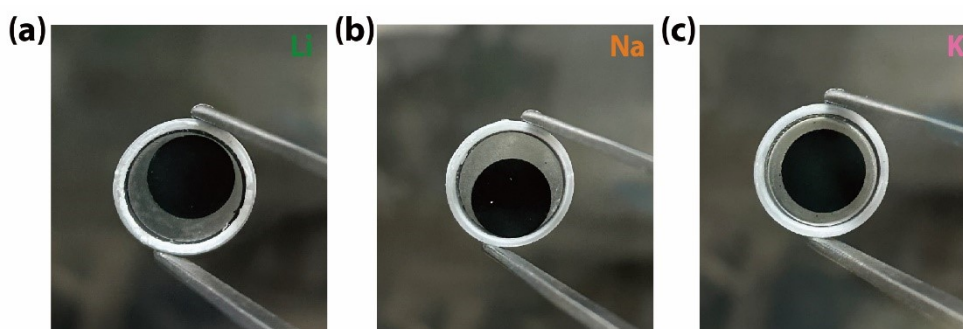
Figure S11. The images of the P(BCz4PZ) cathodes after cycling in Li/Na/K-based dual-ion full cells, respectively.
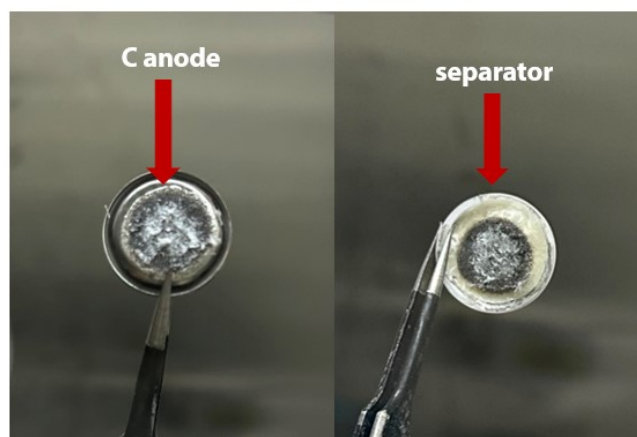
Figure S12. The images of the graphite (C) anode after cycling in Li-based dual-ion full cells.
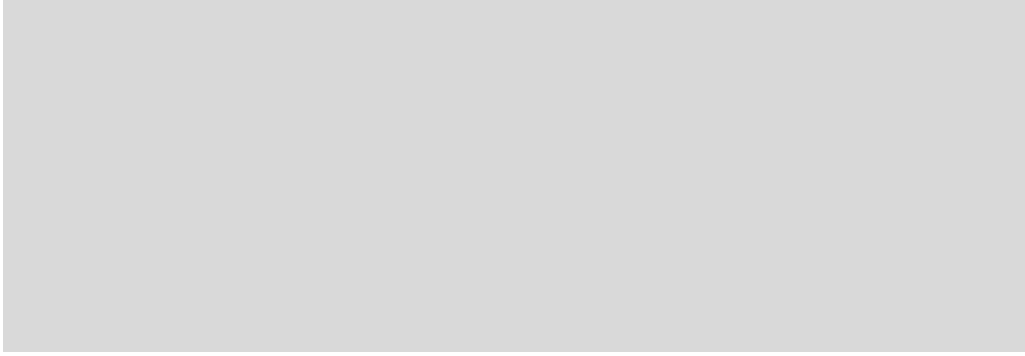
Figure S13. The SEM images of the P(BCz4PZ) electrodes before and after cycling in Na-based half cells.
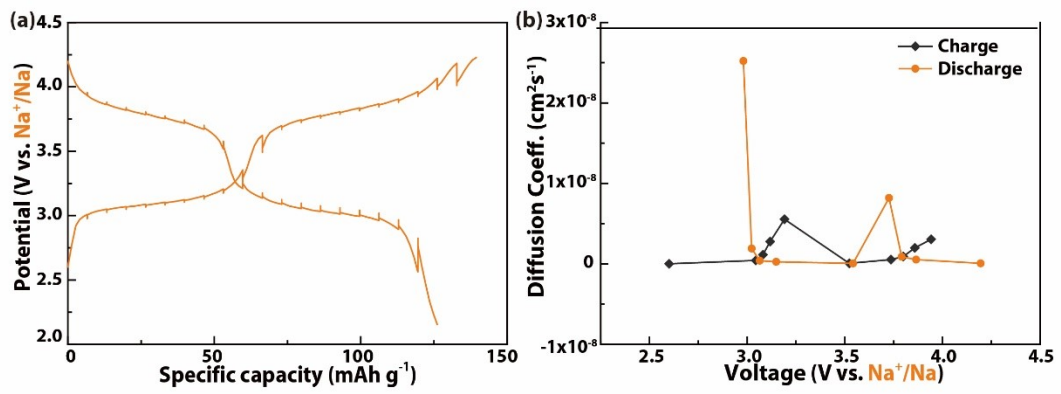
Figure S14. (a) The GITT curves of P(BCz4PZ) in Na-based half cells; (b) The realized ion diffusion coefficient for P(BCz4PZ) in Na-based half cells.
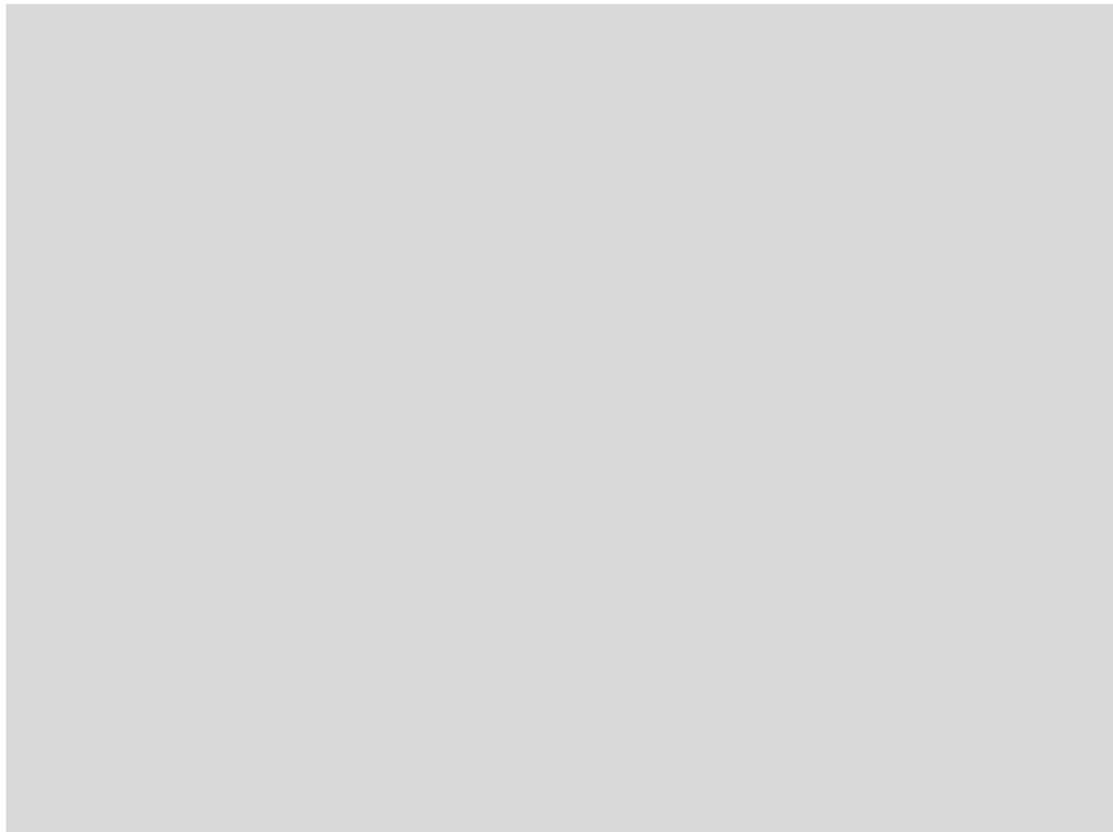
Figure S15. (a)The CV curves of P(BCz4PZ) at different scan rates from 0.1 to 2 mV s^{-1} in Na-based half cells; (b) The linear fitting results of logarithm (log) relationship between peak current and different scan rates; (c) The pseudocapacitance contribution at 0.5 mV s^{-1} for P(BCz4PZ); (d) The pseudocapacitance contribution at various scan rates.
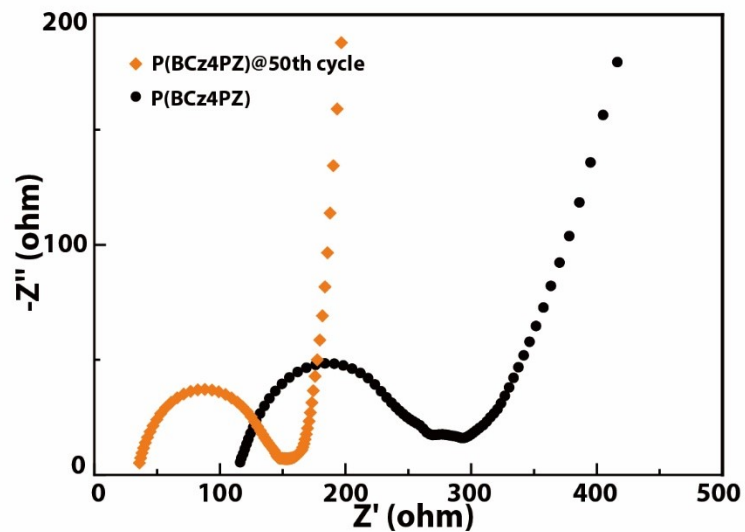
Figure S16. The EIS tests for P(BCz4PZ) before and after cycling in Na-based half cells.
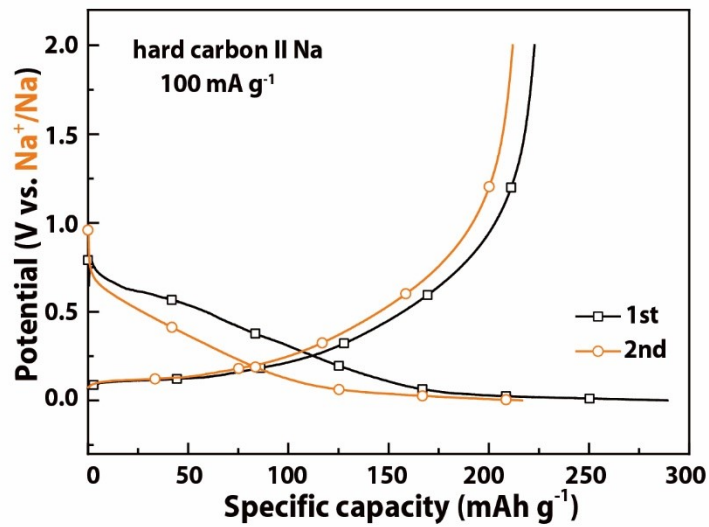
Figure S17. The charge-discharge curves of hard carbon in Na-based half cells in 0.01-2 V.
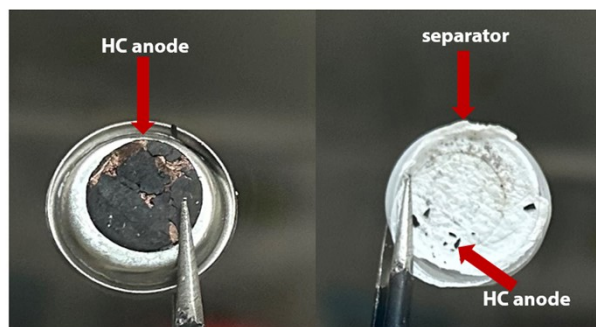
Figure S18. The images of the hard carbon (HC) anode after cycling in Na-based dual-ion full cells.
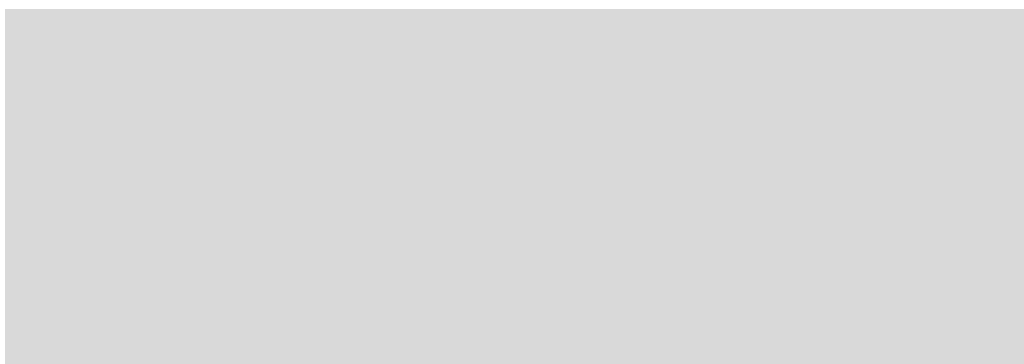
Figure S19. The SEM images of the P(BCz4PZ) electrodes before and after cycling in K-based half cells.
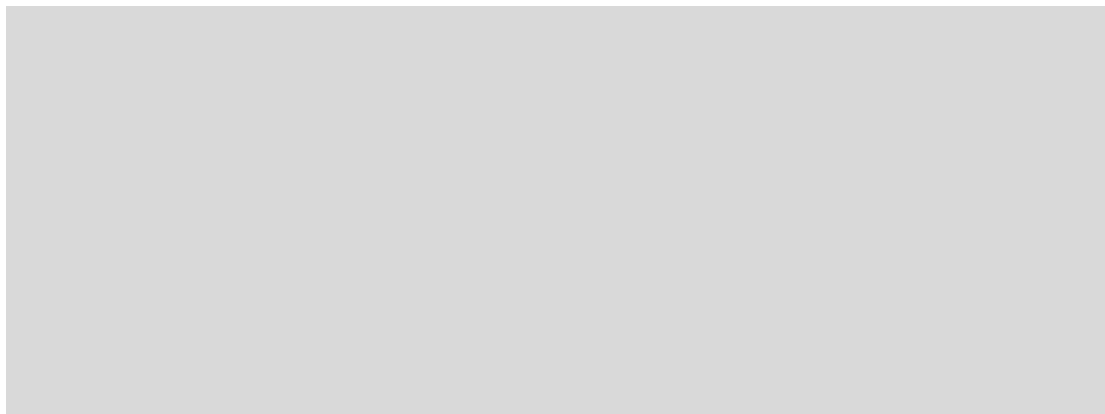
Figure S20. (a) The GITT curves of P(BCz4PZ) in K-based half cells; (b) The realized ion diffusion coefficient for P(BCz4PZ) in K-based half cells.
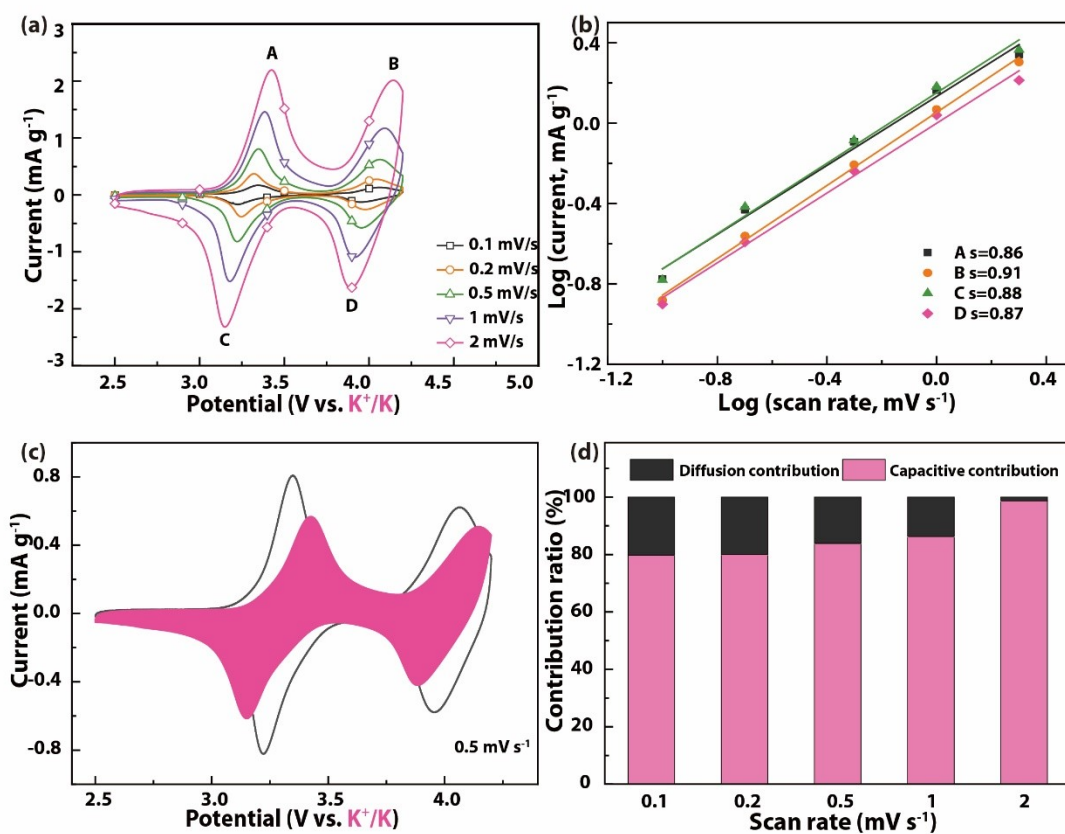
Figure S21. (a)The CV curves of P(BCz4PZ) at different scan rates from 0.1 to 2 mV s⁻¹ in K-based half cells; (b) The linear fitting results of logarithm (log) relationship between peak current and different scan rates; (c) The pseudocapacitance contribution at 0.5 mV s⁻¹ for P(BCz4PZ); (d) The pseudocapacitance contribution at various scan rates.
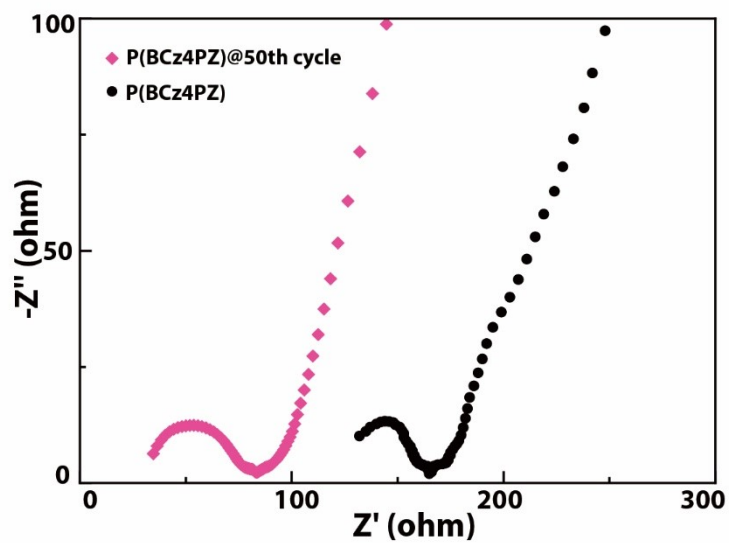
Figure S22. The EIS tests for P(BCz4PZ) before and after cycling in K-based half cells.
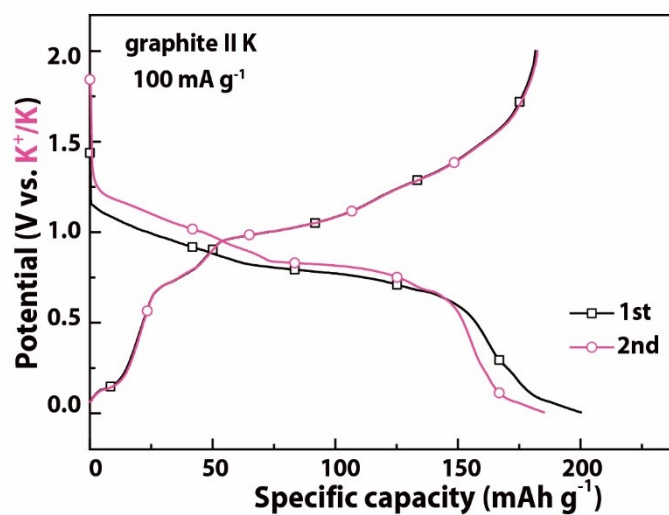
Figure S23. The charge-discharge curves of graphite in K-based half cells in 0.001-2 V.
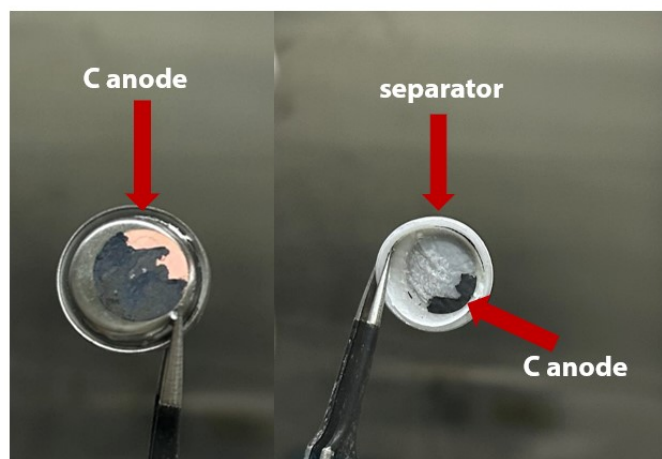
Figure S24. The images of the graphite (C) anode after cycling in K-based dual-ion full cells.

References

1. Y. Yuan, H. Huang, L. Chen and Y. Chen, N,N′-Bicarbazole: A Versatile Building Block toward the Construction of Conjugated Porous Polymers for CO_2 Capture and Dyes Adsorption, *Macromolecules*, 2017, **50**, 4993-5003.
2. L. Yang, X. Li, J. B. Yang, Y. Qu and J. L. Hua, Colorimetric and Ratiometric Near-Infrared Fluorescent Cyanide Chemodosimeter Based on Phenazine Derivatives, *ACS Appl. Mater. Interfaces*, 2013, **5**, 1317-1326.